

Quantum Melting of Spin Ice: Emergent Cooperative Quadrupole and Chirality

Shigeki Onoda and Yoichi Tanaka

Condensed Matter Theory Laboratory, RIKEN, 2-1, Hirosawa, Wako 351-0198, Saitama, Japan
(Received 17 July 2009; revised manuscript received 11 April 2010; published 19 July 2010)

Quantum melting of spin ice is proposed for pyrochlore-lattice magnets $\text{Pr}_2\text{TM}_2\text{O}_7$ (TM = Ir, Zr, and Sn). The quantum superexchange Hamiltonian having a nontrivial magnetic anisotropy is derived on the basis of atomic non-Kramers magnetic doublets. The ground states exhibit a cooperative ferroquadrupole and pseudospin chirality, forming a magnetic analog of smectic liquid crystals. Our theory accounts for dynamic spin-ice behaviors experimentally observed in $\text{Pr}_2\text{TM}_2\text{O}_7$.

DOI: 10.1103/PhysRevLett.105.047201

PACS numbers: 75.10.Jm, 75.10.Dg, 75.30.Kz, 75.50.Ee

It has been a great challenge to realize unconventional spin-liquid states in three-dimensional magnets. It is achieved by preventing a dipole long-range order (LRO) of magnetic moments, which requires appreciable quantum spin fluctuations and geometrical frustration of magnetic interaction [1–4]. The importance of the geometrical frustration is manifest, as in pyrochlore systems [5–8]. In particular, in the dipolar spin ice $R_2\text{Ti}_2\text{O}_7$ ($R = \text{Dy}$ or Ho) [6–8], the rare-earth magnetic moment located at each vertex of the tetrahedrons points either inwards (“in”) to or outwards (“out”) from the center [Fig. 1(a)]. The nearest-neighbor ferromagnetic coupling mainly due to the magnetic dipolar interaction favors macroscopically degenerate “2-in, 2-out” configurations without any LRO, forming a magnetic analog of the water ice [8]. Then, the classical spins are quenched into one of the degenerate ground states [9]. Usually, thermal heating is required for melting the quenched spin ice. Here, we pursue an alternative possibility that quantum fluctuations melt spin ice: the quantum entanglement among degenerate states lifts the macroscopic degeneracy, suppresses the spin-ice freezing, and leads to a distinct ground state.

A realistic approach to quantum melting of spin ice is to choose a rare-earth ion with fewer f electrons and a smaller magnetic moment, e.g., Pr^{3+} . In rare-earth ions with fewer f electrons, the $4f$ wave function is spatially extended [10] and can then be largely overlapped with the O $2p$ orbitals at the O1 site [Fig. 1(a)] in the pyrochlore lattice. Besides, for Pr^{3+} ions, the magnetic dipolar interaction, which is proportional to the square of the moment size, is reduced by an order of magnitude to 0.1 K between the nearest-neighbor sites, in comparison to that for Dy^{3+} ions. Then, the superexchange interaction due to virtual f - p electron transfers, which provides a source of the quantum nature, is expected to play crucial roles in $\text{Pr}_2\text{TM}_2\text{O}_7$ (TM: a transition metal).

Recent experiments on $\text{Pr}_2\text{Sn}_2\text{O}_7$ [11], $\text{Pr}_2\text{Zr}_2\text{O}_7$ [12], and $\text{Pr}_2\text{Ir}_2\text{O}_7$ [13] have shown that the Pr^{3+} ion provides the $\langle 111 \rangle$ Ising moment described by a non-Kramers magnetic doublet. As in spin ice, any magnetic dipole LRO is absent [11–16]. $\text{Pr}_2\text{Ir}_2\text{O}_7$ shows a metamagnetic transition only when the magnetic field is applied in the $[111]$ direc-

tion [14], indicating the ice-rule formation due to a ferromagnetic coupling $J \sim 1.4$ K [14]. On the other hand, the Curie-Weiss temperature T_{CW} is antiferromagnetic for the zirconate [12] and iridate [13], unlike spin ice. The stannate shows a significant level of low-energy short-range spin dynamics [15], which is absent in classical spin ice. Furthermore, the iridate shows the Hall effect at zero magnetic field without magnetic dipole order [14], suggesting an onset of a chiral spin liquid [3] at a temperature $\sim J$ due to quantum fluctuations.

In this Letter, we derive the realistic effective model for Pr $4f$ moments on the pyrochlore lattice. It contains an appreciable quantum nature leading to a cooperative ferroquadrupolar ground state, accompanied by crystal symmetry lowering from cubic to tetragonal and a frustration in the chirality ordering. Our scenario explains unusual magnetic properties observed in $\text{Pr}_2\text{TM}_2\text{O}_7$ suggesting dynamically fluctuating spin ice [14–16].

We start with f^2 configurations for Pr^{3+} forming the tetrahedron centered at the O^{2-} ion (O1) in $\text{Pr}_2\text{TM}_2\text{O}_7$ (Fig. 1). The LS coupling gives the ground-state manifold $3H_4$. Each Pr^{3+} ion is placed in a crystalline electric field (CEF) which has the D_{3d} symmetry about the $\langle 111 \rangle$ direc-

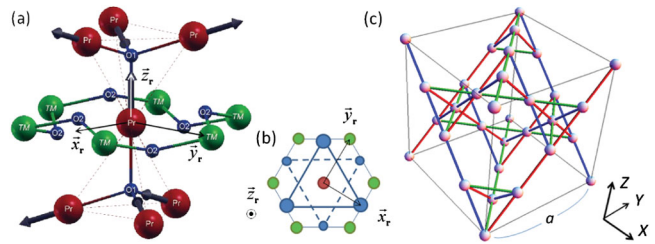


FIG. 1 (color). (a) Pr^{3+} ions (red) form tetrahedrons (dashed lines) centered at O^{2-} ions (O1) (blue), and are surrounded by O^{2-} ions (O2) (blue) in the D_{3d} symmetry as well as by TM ions (green). Each Pr magnetic moment (bold arrow) points to either of the two neighboring O1 sites. (b) The local coordinate frame ($\vec{x}_r, \vec{y}_r, \vec{z}_r$) from the top. Upward and downward triangles of the O^{2-} ions (O2) are located above and below the hexagon of the TM ions. (c) The Pr pyrochlore lattice. The phase $\varphi_{r,r'}$ in Eq. (2) depends on the color of the bonds. The global coordinate frame (X, Y, Z) is also shown.

tion toward the O1 site. It is useful to define the local quantization axis \vec{z}_r as this direction, as well as the x and y axes as \vec{x}_r and \vec{y}_r depicted in Figs. 1(a) and 1(b). The CEF favors $J^z = \pm 4$ configurations for the total angular momentum, which are linearly coupled to $J^z = \pm 1$ and ∓ 2 because of the D_{3d} CEF [17]. This leads to the atomic non-Kramers magnetic ground doublet

$$|\sigma^z\rangle = \alpha|J^z = 4\sigma^z\rangle + \beta\sigma^z|J^z = \sigma^z\rangle - \gamma|J^z = -2\sigma^z\rangle, \quad (1)$$

with small real coefficients β and γ as well as $\alpha = \sqrt{1 - \beta^2 - \gamma^2}$. The pseudospin $\sigma^z = \pm$ represents the direction of the Ising (in or out) magnetic dipole moment, in contrast to the case of a nonmagnetic doublet labeled by the atomic quadrupole moment [18] in materials having other CEF symmetries, PrFe₄P₁₂ [19], UPt₃ [20], and UPd₂Al₃ [21]. For Pr₂Ir₂O₇, the first excited crystal-field level is a singlet located at 168 K and the second is a doublet at 648 K [17]. They are similarly large for Pr₂Sn₂O₇ [15]. These energy scales are 2 orders of magnitude larger than our relevant energy scale $J \sim 1.4$ K. Hence we neglect these CEF excitations.

Now we derive the effective Hamiltonian through the fourth-order strong-coupling perturbation theory. Virtual local f^1 and f^3 states have an energy gain of the Coulomb repulsion U and cost of $2U$, respectively [Fig. 2(a)], where the LS coupling has been ignored in comparison with U . Creating a virtual p hole decreases the energy by the p electron level Δ compared with the f^1 level. The f - p electron transfer is allowed only within the orbital $l_z = 0$ and ± 1 manifolds, whose amplitudes are given by Slater-Koster parameters $V_{pf\sigma}$ and $V_{pf\pi}$ [22], respectively, [Fig. 2(b)]. The local coordinate frames for the nearest-neighbor Pr sites are crucially different; for instance, $\vec{z}_r \cdot \vec{z}_{r'} = -1/3$. The perturbation expansion in $V_{pf\sigma}$ and $V_{pf\pi}$ is then carried out by taking into account the different local coordinate frames and the virtual processes [Fig. 2(c)]. The projection of this superexchange Hamiltonian onto the subspace of doublets [Eq. (1)] leads to the

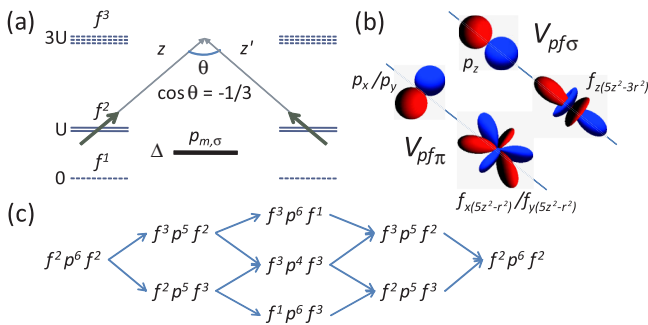


FIG. 2 (color online). (a) Local level scheme for f and p electrons, and the local quantization axes \vec{z}_r and $\vec{z}_{r'}$. (b) f - p transfer integrals. (c) Virtual hopping processes. n (n') and ℓ in the state $f^n p^\ell f^{n'}$ represent the number of f electrons at the Pr site r (r') and that of p electrons at the O1 site.

pseudospin-1/2 Hamiltonian:

$$\mathcal{H}_{\text{eff}} = J \sum_{\langle r, r' \rangle}^{\text{n.n.}} [\sigma_r^z \sigma_{r'}^z + 2\delta(\sigma_r^+ \sigma_{r'}^- + \sigma_r^- \sigma_{r'}^+) + 2q(e^{i\varphi_{r,r'}} \sigma_r^+ \sigma_{r'}^+ + \text{H.c.})], \quad (2)$$

with $\sigma_r^\pm = (\sigma_r^x \pm i\sigma_r^y)/2$ and $(\sigma_r^x, \sigma_r^y, \sigma_r^z) = \vec{\sigma}_r \cdot (\vec{x}_r, \vec{y}_r, \vec{z}_r)$, where $\vec{\sigma}_r$ represents the Pauli matrix for the pseudospin at the site r . We have adopted the simplest gauge where the phase $\varphi_{r,r'}$ takes 0, $2\pi/3$, $-2\pi/3$ depending on the color of the bond directions shown in Fig. 1(c), by rotating the x and y axes by $\pi/12$ from those shown in Figs. 1(a) and 1(b). This phase cannot be fully gauged away, because of the noncollinearity of the $\langle 111 \rangle$ magnetic moments and the threefold rotational invariance of $(r, \vec{\sigma}_r)$ about the $[111]$ axes. Only σ_r^z contributes to the magnetic dipole moment J_r^z , while $\sigma_r^{x,y}$ the atomic quadrupole moment $J_r^{x,y}$, as can be shown by direct calculations. For a realistic case $-0.37 \lesssim V_{pf\pi}/V_{pf\sigma} \lesssim -0.02$, the Ising coupling J between the nearest-neighbor pseudospins is found to be positive, i.e., antiferroic. This indicates the “ferromagnetic” coupling between the nearest-neighbor $4f$ magnetic moments because of the tilting of the local z axes, $\vec{z}_r \cdot \vec{z}_{r'} = -1/3$. Then, it can provide a source of the ice-rule formation. The D_{3d} CEF creates two additional quantum-mechanical interactions: the pseudospin-exchange and pseudospin-nonconserving terms. Their coupling constants δ and q are insensitive to $U/V_{pf\sigma}$ and $\Delta/V_{pf\sigma}$ but strongly depend on β and γ . Figure 3(a) shows δ and q as functions of β for the trigonal CEF by keeping the ratio $\gamma/\beta = 3$. Henceforth, we adopt rough estimates $U/V_{pf\sigma} = 5$, $\Delta/V_{pf\sigma} = 4$, and $V_{pf\pi}/V_{pf\sigma} = -0.3$ from first-principles calculations (published elsewhere), and $\beta = 7.5\%$ and $\gamma = 3\beta$ from the CEF analysis based on

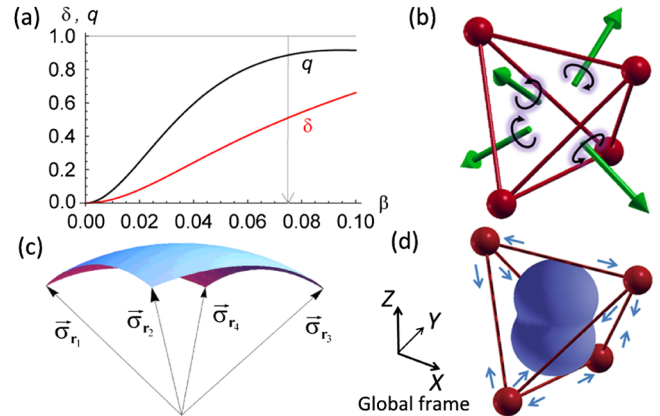


FIG. 3 (color online). (a) Coupling constants δ and q versus β ($= \gamma/3$). The arrow points to the experimentally estimated value of β [17]. (b) Outward normal vectors (green arrows) of the surfaces of the tetrahedron, used to define the chirality κ_T . (c) Solid angle subtended by four pseudospins $\vec{\sigma}_r$. (d) Distribution of the tetrahedral magnetic moment \vec{M}_T in the cooperative ferroquadrupolar state ($\langle Q_T^{ZZ} \rangle > 0$). The arrows represent the lattice deformation linearly coupled to Q_T^{ZZ} .

inelastic neutron-scattering experiments [17]. Then, we obtain $\delta \sim 0.51$ and $q \sim 0.89$, indicating the appreciable quantum nature. The two couplings play crucial roles in inducing a cooperative ferroquadrupolar order instead of classical spin ice [8] or the U(1) spin liquid [23].

A mean-field analysis [5] on Eq. (2) yields two distinct states. (i) Magnetic dipolar states characterized by a nonzero $\langle \sigma_r^z \rangle$ have the lowest energy $-2J$ per tetrahedron at the wave vector $\mathbf{q} = \frac{2\pi}{a}(hhl)$ with a being the side length of the unit cube [Fig. 1(c)]. (ii) A quadrupolar state with a nonzero $\langle \sigma_r^{x,y} \rangle$ has the energy $-2(\delta + 2q)J$ at $\mathbf{q} = 0$ for $\delta, q > 0$. Thus, for $\delta + 2q > 1$ as in our case, the atomic quadrupole moment $\sigma_r^{x,y}$ should form the LRO without any dipole LRO. However, we will show below that the ground state is further replaced with a cooperative ferroquadrupolar state because of the quantum interplay between atomic dipoles σ_r^z and quadrupoles $\sigma_r^{x,y}$.

First let us solve Eq. (2) on a single tetrahedron. The similar analysis on a distinct model for $\text{Tb}_2\text{Ti}_2\text{O}_7$ [24] has been employed to discuss the resonating-valence-bond-singlet quantum spin ice [25]. With increasing β and thus γ from 0, three classical levels corresponding to the “2-in, 2-out,” “3-in, 1-out”/“1-in, 3-out” ($\Delta E = 2J$), and “4-in”/“4-out” ($\Delta E = 8J$) configurations are split to three doublets, three triplets, and one singlet. In our case, the ground-state manifold has the E_g symmetry with the double degeneracy $\chi = \pm$ as described as $|\Psi_\chi^s\rangle = (c_2/\sqrt{6})\sum_{\tau=\pm}(e^{i(2\pi/3)\chi}|\tau X\rangle + e^{-i(2\pi/3)\chi}|\tau Y\rangle + |\tau Z\rangle) + c_4|4\chi\rangle$ with real coefficients c_2 and c_4 . Here, $|+4\rangle/|-4\rangle$ represents the “4-in”/“4-out” configuration, while $|\pm X\rangle, |\pm Y\rangle$, and $|\pm Z\rangle$ denote the “2-in, 2-out” having the net magnetic dipole moment $\vec{M}_T = M_0 \sum_r \sigma_r^z \vec{z}_r$, pointing to the $\pm X, \pm Y$, and $\pm Z$ directions of the global coordinate frame, respectively. We have introduced the moment amplitude $M_0 = g_J \mu_B (4\alpha^2 + \beta^2 - 2\gamma^2) \approx 2.9 \mu_B$ with the Landé factor $g_J = 4/5$. The sign $\chi = \pm$ represents the net pseudospin chirality of the tetrahedron, $\kappa_T = \frac{1}{2} \sum_{\mathbf{r}_1, \mathbf{r}_2, \mathbf{r}_3} \vec{\sigma}_{\mathbf{r}_1} \cdot \vec{\sigma}_{\mathbf{r}_2} \times \vec{\sigma}_{\mathbf{r}_3}$, through the relation $\langle \Psi_\chi^s | \kappa_T | \Psi_{\chi'}^s \rangle = \sqrt{3} c_2^2 \delta_{\chi, \chi'}$. Here, the summation over the sites $\mathbf{r}_1, \mathbf{r}_2, \mathbf{r}_3$ on the tetrahedron T is taken so as they appear counterclockwise about the outward normal to the plane spanned by the three sites [Fig. 3(b)]. This κ_T is associated with the solid angle subtended by the four pseudospins [Fig. 3(c)]. Note that the “2-in, 2-out” singlet state with the A_{1g} symmetry [25], $\sum_{\tau=\pm} (|\tau X\rangle + |\tau Y\rangle + |\tau Z\rangle)/\sqrt{6}$, is located at a high energy $\Delta E \sim 7J$. The triply degenerate first excited states consist of only “3-in, 1-out” and “1-in, 3-out”, and are located at $\Delta E \sim J$. In fact, any eigenstate of the single-tetrahedron Hamiltonian is described by either “3-in, 1-out” and “1-in, 3-out” configurations or “2-in, 2-out” and “4-in”/“4-out” configurations. Therefore, quantum effects of creating “3-in, 1-out” and “1-in, 3-out” from the “2-in, 2-out” cannot be taken into account in the single-tetrahedron analysis.

To overcome this drawback, we numerically solve the model for the 16-site ($N = 16$) cubic cluster with the

periodic boundary condition [Fig. 1(c)]. It is found that the ground states have a sixfold degeneracy labeled by the inversion (I) even(+)/odd(-) and the wave vector $\mathbf{k}_X = (\frac{2\pi}{a}, 0, 0)$, $\mathbf{k}_Y = (0, \frac{2\pi}{a}, 0)$, or $\mathbf{k}_Z = (0, 0, \frac{2\pi}{a})$ with the energy $\sim -8.825J$ per tetrahedron. The states associated with \mathbf{k}_i have a cooperative quadrupole moment defined on each tetrahedron, $\langle Q_T^{ij} \rangle = 0.0387M_0^2$, where $Q_T^{ij} = 3M_T^i M_T^j - \vec{M}_T^2 \delta_{ij}$ with $i, j = X, Y, Z$. Namely, the net magnetic moment \vec{M}_T in each tetrahedron T points, for instance, to the $\pm Z$ directions with a higher probability than to the $\pm X$ and $\pm Y$ [Fig. 3(d)]. Such ferroquadrupole order spontaneously breaking the threefold rotational invariance about the [111] axes can occur in the thermodynamic limit. This ferroquadrupole moment Q_T^{ij} linearly couples to a lattice vibration: the four ferromagnetic bonds and the two antiferromagnetic bonds should be shortened and expanded, respectively, leading to a crystal symmetry lowering from cubic to tetragonal accompanied by a compression in the direction of the ferroquadrupole moment [Fig. 3(d)]. This state shows both axial alignments of magnetic dipoles and a broken translational symmetry, and can then be classified into a magnetic analog of a smectic (or crystalline) phase of liquid crystals [26]. Such magnetic quadrupole correlations in $\text{Pr}_2\text{TM}_2\text{O}_7$ could be probed by NMR experiments.

Next, we calculate the magnetic dipole correlation, $S(\mathbf{q}) = \frac{M_0^2}{N} \sum_{\mathbf{r}, \mathbf{r}', i, j} (\delta_{ij} - \frac{q_i q_j}{|q|^2}) z_r^i z_{r'}^j \langle \sigma_r^z \sigma_{r'}^z \rangle_{\text{ave}} e^{iq \cdot (\mathbf{r} - \mathbf{r}')}$, averaged over the sixfold degenerate ground states. This quantity is relevant to the neutron-scattering intensity integrated over the low-energy region below the crystal-field excitations from the atomic ground doublet Eq. (1). Note that neutron spins do not couple to σ_r^\pm which represents the atomic quadrupole. Figure 4(a) shows the profile of $S(\mathbf{q})$ for $\mathbf{q} = \frac{2\pi}{a}(hhl)$. It exhibits intense peaks at (001) and (003), weaker peaks at $(\frac{3}{4}, \frac{3}{4}, 0)$, and the minimum at (000), as in the dipolar spin ice [8], though the peaks are broadened by the quantum fluctuations in this ferroquadrupolar state. Besides, the nonzero q term in the Hamiltonian partially violates the ice rule and eliminates the pinch-point singularity [27,28] observed at (111) and (002) in spin ice [29], which should be examined by large system-size calculations. Note that our magnetic profile reproduces powder neutron-scattering results on $\text{Pr}_2\text{Sn}_2\text{O}_7$ [15] that reveal the enhanced low-energy short-ranged intensity at $q \sim \frac{2\pi}{a} \sim 0.5 \text{ \AA}^{-1}$ with a shoulder at $q \sim \frac{6\pi}{a}$ [Fig. 4(b)]. This experiment also shows a saturation of the quasielastic peak width $\sim 0.1 \text{ meV} \sim J$ at 0.2 K [15]. Such a large spin relaxation rate can be attributed to the appreciable quantum nature: large δ and q in Eq. (2). These agreements support our scenario of quantum melting of spin ice.

Now we concentrate on the ground states having the quadrupole moment $\langle Q_T^{ZZ} \rangle > 0$ and the associated wave vector \mathbf{k}_Z . The magnetic susceptibility is finite in the ferroquadrupolar state, as seen from the slope of the magnetization curve along the $\langle 111 \rangle$ direction in Fig. 4(c). This

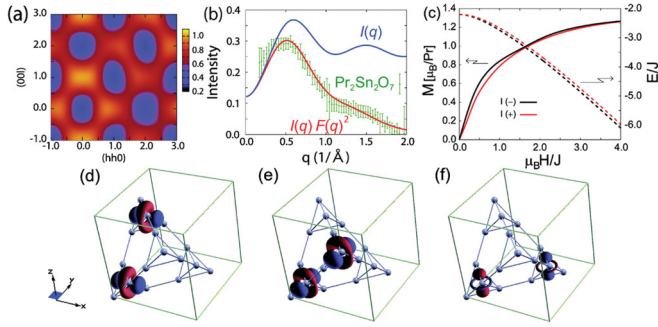


FIG. 4 (color). (a) $S(\mathbf{q})/M_0^2$ constructed from the local, nearest-neighbor, and second-neighbor correlations. (b) The theoretical curve (red) $I(q)F(q)^2$ with the form factor $F(q)$ and the powder neutron-scattering data (green) on $\text{Pr}_2\text{Sn}_2\text{O}_7$ at 1.4 K [15]. $I(q)$ (blue curve) is the angle average of $S(\mathbf{q})/M_0^2$. (c) The magnetizations (left) and energies (right) per site for the I -odd(-) ground state and the I -even(+) state under the magnetic field $\vec{H} \parallel \langle 111 \rangle$. (d–f) Quadrupole correlations $\langle Q_T^{ii} Q_{T'}^{jj} \rangle$ between the tetrahedrons T and T' displaced by $\mathbf{r} = \mathbf{r}_X$ (d), \mathbf{r}_Y (e), and \mathbf{r}_Z (f) in the cooperative ferroquadrupolar state with the wave vector \mathbf{k}_Z and $\langle Q_T^{ZZ} \rangle \neq 0$. The matrix $\langle Q_T^{ii} Q_{T'}^{jj} \rangle$ in i, j has been diagonalized to yield two orthogonal forms of quadrupoles, $Q_{r\mu} = \sum_i \lambda_{r\mu}^i Q_T^{ii}$ ($\mu = 1, 2$). The shape of Q_{r1} showing the dominant correlation amplitude is shown. Red (blue) regions represent positive (negative) values of Q_{r1} .

indicates a negative T_{CW} as found in $\text{Pr}_2\text{Zr}_2\text{O}_7$ [12] and $\text{Pr}_2\text{Ir}_2\text{O}_7$ [14], and the absence of an internal magnetic field as in $\text{Pr}_2\text{Ir}_2\text{O}_7$ [16]. The magnetic field lifts the degeneracy due to the I symmetry. The ground-state (I -odd) magnetization shows a small step or dip around $\mu_B H/J \sim 1.5$, in comparison with that of the I -even excited state. This indicates that the structure develops upon cooling. This agrees with the experimental observation on $\text{Pr}_2\text{Ir}_2\text{O}_7$: $M \sim 0.8\mu_B$ at the metamagnetic transition $\mu_B H_c/J \sim 1.3$ with $J \sim 1.4$ K [14].

Finally we spatially resolve the multipolar correlations within the cubic unit cell. Figures 4(d)–4(f) represent quadrupole correlations $\langle Q_T^{ii} Q_{T'}^{jj} \rangle$ between the tetrahedrons T and T' displaced by $\mathbf{r}_X = (0, \frac{a}{2}, \frac{a}{2})$, $\mathbf{r}_Y = (\frac{a}{2}, 0, \frac{a}{2})$, and $\mathbf{r}_Z = (\frac{a}{2}, \frac{a}{2}, 0)$, respectively. There exist dominant ferroquadrupolar correlations shown in Figs. 4(d) and 4(e), both of which favor ferroquadrupole moments along the Z direction. They prevail over subdominant antiferroquadrupole correlations shown in Fig. 4(f), and are responsible for the ferroquadrupole order $\langle Q_T^{ZZ} \rangle \neq 0$. On the other hand, the chirality correlation $\langle \kappa_T \kappa_{T'} \rangle$ is weakly ferrochiral between the tetrahedrons shown in Figs. 4(d) and 4(e), while it is strongly antiferrochiral between those shown in Fig. 4(f). This points to a geometrical frustration suppressing the chirality LRO in each fcc sublattice of the diamond lattice formed by the tetrahedrons. Further studies are required to examine the possibility of a chiral spin liquid [3]. The broken time-reversal symmetry without magnetic dipole LRO, reported in $\text{Pr}_2\text{Ir}_2\text{O}_7$ [14], might be detected even in insulating magnets such as $\text{Pr}_2\text{Zr}_2\text{O}_7$

and $\text{Pr}_2\text{Sn}_2\text{O}_7$ through magneto-optical Kerr-effect measurements.

The proposed scenario of quantum melting of spin ice explains magnetic properties observed in $\text{Pr}_2\text{TM}_2\text{O}_7$. The effects of coupling of localized f electrons to conduction electrons on the transport properties are left for a future study. The orbital motion of conduction electrons can flip the pseudospin 1/2. This could be an origin of the resistivity minimum observed in $\text{Pr}_2\text{Ir}_2\text{O}_7$ [13].

The authors thank S. Nakatsuji, Y. Machida, Y. B. Kim, C. Broholm, L. Balents, K. Matsuhira, and D. MacLaughlin for discussions. The work was supported by Grants-in-Aid for Scientific Research under No. 19052006, No. 20029006, and No. 20046016 from the MEXT of Japan and No. 21740275 from the JSPS.

- [1] P. W. Anderson, *Phys. Rev.* **102**, 1008 (1956).
- [2] P. W. Anderson, *Mater. Res. Bull.* **8**, 153 (1973).
- [3] X. G. Wen, F. Wilczek, and A. Zee, *Phys. Rev. B* **39**, 11 413 (1989).
- [4] P. A. Lee, *Science* **321**, 1306 (2008).
- [5] J. N. Reimers, A. J. Berlinsky, and A. C. Shi, *Phys. Rev. B* **43**, 865 (1991).
- [6] M. J. Harris *et al.*, *Phys. Rev. Lett.* **79**, 2554 (1997).
- [7] A. P. Ramirez *et al.*, *Nature (London)* **399**, 333 (1999).
- [8] S. T. Bramwell and M. J. P. Gingras, *Science* **294**, 1495 (2001).
- [9] C. Castelnovo, R. Moessner, and S. L. Sondhi, *Phys. Rev. Lett.* **104**, 107201 (2010).
- [10] J. Rossat-Mignod, in *Proceedings of the Nato Advanced Study Institute on Systematics and the Properties of the Lanthanides*, edited by S. P. Sinha (Reidel, Dordrecht, 1983).
- [11] K. Matsuhira *et al.*, *J. Phys. Soc. Jpn.* **71**, 1576 (2002).
- [12] K. Matsuhira *et al.*, *J. Phys. Conf. Ser.* **145**, 012 031 (2009).
- [13] S. Nakatsuji *et al.*, *Phys. Rev. Lett.* **96**, 087204 (2006).
- [14] Y. Machida *et al.*, *Nature (London)* **463**, 210 (2010).
- [15] H. D. Zhou *et al.*, *Phys. Rev. Lett.* **101**, 227204 (2008).
- [16] D. E. MacLaughlin *et al.*, *Physica (Amsterdam)* **404B**, 667 (2009).
- [17] Y. Machida, Ph.D. thesis, Kyoto University, 2006.
- [18] D. L. Cox, *Phys. Rev. Lett.* **59**, 1240 (1987).
- [19] Y. Aoki *et al.*, *Phys. Rev. B* **65**, 064446 (2002).
- [20] R. Joynt and L. Taillefer, *Rev. Mod. Phys.* **74**, 235 (2002).
- [21] A. Grauel *et al.*, *Phys. Rev. B* **46**, 5818 (1992).
- [22] R. R. Sharma, *Phys. Rev. B* **19**, 2813 (1979).
- [23] M. Hermele, M. P. A. Fisher, and L. Balents, *Phys. Rev. B* **69**, 064404 (2004).
- [24] J. S. Gardner *et al.*, *Phys. Rev. Lett.* **82**, 1012 (1999).
- [25] H. R. Molavian, M. J. P. Gingras, and B. Canals, *Phys. Rev. Lett.* **98**, 157204 (2007).
- [26] P. G. de Gennes and J. Prost, *The Physics of Liquid Crystals* (Clarendon, Oxford, 1993), 2nd ed.
- [27] S. V. Isakov *et al.*, *Phys. Rev. Lett.* **93**, 167204 (2004).
- [28] C. L. Henley, *Phys. Rev. B* **71**, 014424 (2005).
- [29] D. J. P. Morris *et al.*, *Science* **326**, 411 (2009); T. Fennell *et al.*, *Science* **326**, 415 (2009).